Arabian Journal of Chemistry (2017) **10**, S439–S449

King Saud University

Arabian Journal of Chemistry

www.ksu.edu.sa
www.sciencedirect.com

ORIGINAL ARTICLE

Some physico-chemical properties and catalytic activity of sulfate ion supported on WO_3/SnO_2 catalyst

M.N. Alaya *, M.A. Rabah

Chemistry Department, Faculty of Science, University of Aleppo, Syria

Received 1 December 2011; accepted 4 October 2012
Available online 13 October 2012

KEYWORDS

$SO_4/WO_3/SnO_2$;
TG-DTA;
XRD;
FTIR;
Surface acidity;
Esterification reaction

Abstract Solid acid catalyst 15 wt%WO_3/SnO_2 was synthesized and loaded with 15 wt%SO_4. The obtained catalyst was calcined at 400, 500, 650 and 800 °C. The prepared catalysts were characterized by TG-DTA, XRD, FTIR and N_2 adsorption at −196 °C. The surface acidity was measured by non aqueous potentiometric titration and FT-IR spectra of chemisorbed pyridine. The catalytic performance was evaluated on the esterification of propionic acid with *n*-butanol in liquid phase. The TG-DTA analysis shows that the decomposition of sulfate species occurred at > 500 °C. XRD measurements showed that WO_3 dispersed completely on the surface of SnO_2 and that the sulfating of WO_3/SnO_2 tends to hinder the crystallization of SnO_2. The specific surface area, total pore volume and micropore volume are increased with increasing thermal treatment up to 500 °C, and then decreased gradually with a further increase in calcination temperature. The prepared catalysts possess very strong acid sites and contain both Brønsted and Lewis acid sites. The total surface acidity decreased with raising of the calcination temperature. The highest conversion of propionic acid was for 400 °C product, and decreased with an increase in calcination temperature. The effect of the reaction parameters, i.e., time of reaction, reaction temperature, and reactant molar ratio and the weight of the catalyst were also studied. The reaction obeys the second order kinetic equation with respect to propionic acid concentration. Brønsted and Lewis acid sites appeared to be needed for catalytic activity in *n*-butyl propionate formation.

1. Introduction

Many reactions in synthetic organic chemistry are acid-catalyzed reactions. These reactions include esterification, etherification, hydration, hydrolysis, alkylation, isomerization and others. Liquid-phase esterification is an important method for producing various esters. The esters are used in the manufacturing of solvents, plasticizers, plastics, leather, perfumes, medicine. . .etc. (Ali et al., 2007; Lilja et al., 2002). Conventional

* Corresponding author. Tel.: +963 21 5740071.
E-mail address: mnalaya@myway.com (M.N. Alaya).
☆ Peer review under responsibility of King Saud University.

Production and hosting by Elsevier

http://dx.doi.org/10.1016/j.arabjc.2012.10.004
1878-5352

mineral acids were used as catalysts in esterification reactions. These homogeneous catalysts suffer from several disadvantages, such as their miscibility with the reaction medium, which causes separation problems, the existence of side reactions, corrosion of the equipment and the need to deal with acidic wastes (Liu and Tan, 2001). The growing awareness of the unacceptability of these liquid catalysts and the resulting legislation give a major impetus to the search for cleaner technology. Cleaner technology could be possible by making use of environment friendly heterogeneous catalysts involving the use of solid acids (Sharma et al., 2004).

Metal oxides, mixed oxides, cation exchange resins and zeolites were the most used solid acids (Tanabe, 1981). In the last decade, it is found that the loading of some metal oxides with sulfate ion or acidic high valence metal oxides such as WO_3 and MoO_3 causes an increase in the acidity of the catalyst and produces superacids (Yamaguchi, 1990; Arata, 1996). Also, metal oxides and resins may be supported by heteropoly acids or sulfonic acid and show a high activity for esterification reactions (Khder, 2008; Parida and Mallick, 2007; Bahatt and Patel, 2005; Ali et al., 2007; Xi and Cao, 2010). The textural properties, surface acidity and catalytic activity of the catalyst depend on the percentage of loading, calcination temperature and the method of preparation (Khder et al., 2008; Sharma et al., 2004).*n*-butyl propionate ester was synthesized by the catalytic esterification of 1-butanol with propionic acid. The catalysts used for this reaction include sulfuric acid and $AlCl_3$ (Rao et al., 1979), ion-exchange resins (Dakshinamurty et al., 1984; Liu et al., 2006; Lee et al., 2002; Ali et al., 2007; Xi and Cao, 2010), 12-tungstosilicic acid on hydrous zirconia (Bahatt and Patel, 2005) and fibrous polymer-supported sulfonic acid (Lilja et al., 2005).

Many papers concerning the preparation, characterization and catalytic activity of WO_3–SnO_2 catalysts were reported (Ai, 1984; Arata and Hino, 1993; Maksimov et al., 2000; Arata et al., 2000; Ma et al., 2000; Hino et al., 2006, 2007; Pimtong-Ngam et al., 2007; Khder and Ahmed, 2009; Shouli et al., 2010; Sarkar et al., 2010). But, no papers concerning sulfated WO_3/SnO_2 catalysts were found.

In the present investigation, we have prepared a 15 wt%WO_3/SnO_2 support loading it with 15 wt%SO_4. The effect of calcination temperature on the structural and textural properties, as well as on the surface acidity was investigated. The catalytic activities of the obtained catalysts were tested by esterification of propionic acid (PA) with *n*-butanol (B). Further, the effect of various reaction parameters on the catalytic activity was also studied.

2. Experimental

2.1. Materials

Pure tin oxide gel was prepared by a dropwise addition of ammonia solution (10 wt%) to 0.5 M solution of $SnCl_4.5H_2O$ (Riedel–deHaen) with vigorous stirring for 4 h, the final pH of the gel was adjusted to 8. The gel was left overnight washed by decantation with 1 wt% ammonium acetate solution (Matsuhashi et al., 1990) until all chloride ions were eliminated (silver nitrate test), then washed with double distilled water and finally dried at 120 °C. Appropriate amount of ammonium paratungstate (APT) solution (30 g/L) (Prolabo) was added to the dry tin hydroxide gel, to obtain 15 wt%WO_3 loading, with vigorous stirring for 4 h. The product was left overnight then dried at 120 °C. The WO_3/SnO_2 support was sulfated by the addition of an appropriate amount of 1 M H_2SO_4 solution, to obtain 15 wt%SO_4 loading, with stirring for 4 h, followed by drying at 120 °C for 24 h. The prepared catalyst was calcined in air at 400, 500, 650 and 800 °C for 4 h. The samples were designated as SWS-*x*, where *x* represents the calcination temperature.

2.2. Techniques

Thermal analysis (TG-DTA) of uncalcined sample was carried in air atmosphere using Linseis Thermal Analyzer, Type STA PT-1600 (Germany). A weight of ~45 mg was placed in a crucible of 100 μL capacity. The run was followed between 25 and 800 °C at a heating rate of 10°/min.

The X-ray powder diffractograms, of the samples calcined at 500 and 800 °C were recorded on Philips Diffractometer Type PW (1830). The pattern was obtained with Ni-filtered CuKα radiation (λ = 1.5418 Å) at 40 kV and 30 mA, with a scanning speed of 1° in 2θ, and a scanning range 2θ of 20–70°. The spacing *d* corresponding to 2θ of the peaks was calculated and correlated with that of ASTM to determine the phases existing.

The FT-IR spectra of the samples were recorded using Jasco FT-IR-460 spectrophotometer in the range of 1200–1700 cm^{-1}, at a resolution of 4 cm^{-1}; by mixing 0.005 g of the sample with 0.1 g KBr in 30 mm diameter self supporting disks were used.

The textural properties of all the samples were determined from the analysis of the data of nitrogen adsorption at 77 K, using Gemini III 2375 Surface Area Analyzer apparatus. Prior to any adsorption measurement, the sample was degassed at 200 °C for 6 h under a reduced pressure of 10^{-4} Torr.

The total acidity of the solid samples was measured by means of potentiometric titration method (Rao et al., 2006; Bennaradi et al., 2007). The dry solid (0.1 g) was suspended in 10 mL acetonitrile (Lab-Scan), and agitated for 3 h. Then, the suspension was titrated with 0.1 N *n*-butylamine (Merck) at 0.05 mL/min. The electrode potential variation was measured with Inolab Digital pH–mV model using a double junction electrode. The nature of acid sites presented on the surface of the catalyst was determined with FTIR transmission spectra of adsorbed pyridine (Scharlau) at the range of 1200–1700 cm^{-1}. Prior to the pyridine adsorption (Khder et al., 2008; Khder and Ahmed, 2009), the samples were degassed at 200 °C for 3 h under high vacuum followed by suspending in a dried pyridine. Then, the excess pyridine was removed by evaporation at 70 °C.

The catalytic activity of the prepared catalysts was tested for the esterification of propionic acid (Merck) with *n*-butanol (SRL). The esterification reaction was carried out in a 100 mL flat-bottomed flask, equipped with a reflux condenser, containing a stirring mixture of propionic acid (0.05 M), *n*-butanol (0.10 M) and the catalyst (0.2 g). The stirring rate in all the experiments was 600 rpm. The reaction mixture was stirred at 110 °C for 4 h. After that, the reaction mixture was immediately filtered and quenched to stop the reaction. Liquid samples (0.5 mL) were withdrawn and the amount of unreacted acid was analyzed by titration with 0.1 N NaOH. The effects of reaction temperature, weight of the catalyst, the initial molar ratio between the acid and alcohol, calcination temperature and the time of reaction were studied.

3. Results and discussion

3.1. Thermal analysis

Fig. 1 shows the TG-DTA curves of the dried catalyst. The TG curve shows four characteristic steps at 50–200, 200–480, 480–560 and 560–770 °C with a weight loss of 4.2, 2.0, 7.0 and 4.2 wt%, respectively. These steps were accompanied with endothermic effects in DTA curve, in which their peaks appeared at 135.2, 331, 530.7 and ~662 °C, respectively. The first two thermal effects are due to the desorption of physically adsorbed water, loss of chemically bonded water and decomposition of APT with the evolution of ammonia, and the second two endothermic effects are due to the decomposition of sulfate species bonded to the support surface (Gutierrez-Baez et al., 2004; Khder et al., 2008). The DTA curve does not show any exothermic signals at 300–450 °C which characterize the formation of crystalline phases of WO_3 and SnO_2. This indicates that the addition of APT and sulfate ions to tin hydroxide gel would hinder the crystallization of SnO_2, and WO_3 is highly dispersed on SnO_2 surface (Gutierrez-Baez et al., 2004; Khder and Ahmed, 2009).

3.2. X-ray diffraction

The X-ray diffractograms of SWS samples calcined at 500 and 800 °C in the range $2\theta = 20–70°$ are shown in Fig. 2. It is observed that the XRD curve for SWS-500 product is poorly crystalline which means that loading of SnO_2 with WO_3 and SO_4 inhibits the crystallization of SnO_2. The XRD pattern of SWS-800 sample shows the characteristic peaks of tetragonal cassiterite structure at $2\theta = 26.6°$, 33.8° and 51.9° (JCPDS No. 41–1445). This would suggest that the crystallization and sintering of SnO_2, is due to the loss of sulfate species bonded to the support (Zhang and Gao, 2004). The characteristic peaks of crystalline WO_3 phase at $2\theta = 23.12°$, 23.59° and 24.38° (JCPDS No. 46–1096) were not observed, which means that WO_3 crystals were transformed into very small crystals or dispersed completely over SnO_2 (Khder and Ahmed, 2009). These results are in good agreement with TG-DTA results. The mean crystallite size calculated from the broadening of the strongest peak of SnO_2, peak (110) at $2\theta = 26.6°$, and based on Scherrer equation, is $d = 6.95$ nm. This value indicates that the prepared catalyst is of nanocrystalline structure.

3.3. FT-IR spectra

The FT-IR spectra of the calcination products of SWS catalyst are shown in Fig. 3. The spectra show vibration bands at 523 and 622 cm^{-1}which are assigned to the stretching vibration of O–Sn–O of tin oxide framework (Zhang and Gao, 2004; Salavati-Niasari et al., 2010). The bands at ~820 and 985 cm^{-1} identify the stretching vibrations of O–W–O and W═O, respectively (Khder and Ahmed, 2009; Sarkar et al., 2010). The spectra show bands in the range of 1025–1400 cm^{-1} attributed to chelating bidentate sulfate on the support (Yamaguchi et al., 1986; Khder and Ahmed, 2009). So, the peaks at 1029, 1157 and 1394 cm^{-1} are assigned to asymmetric stretching vibrations of S═O and S–O (Sohn et al., 2006). The bands around 1618 cm^{-1} are attributed to the bending vibration of water (Cui et al., 2007). The spectra reveal that raising the calcination temperature to >500 °C causes disappearance of the characteristic bands of S═O and S–O due to the decomposition of sulfate species bonded to the support, which is in good agreement with thermal analysis results.

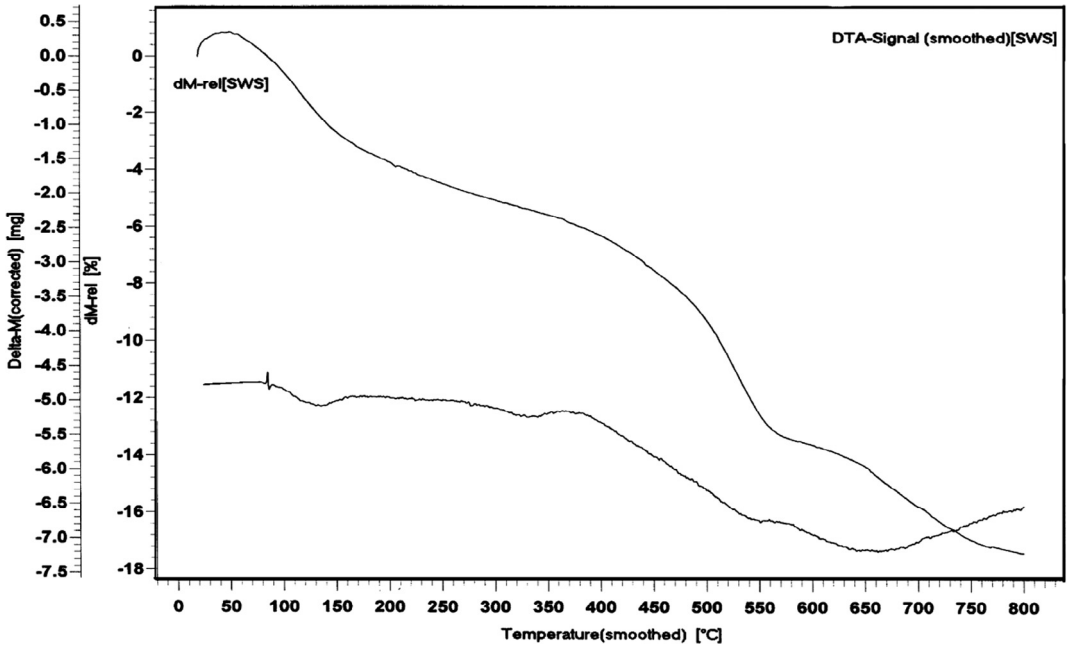

Figure 1 The TG and DTA curves of the dried prepared samples.

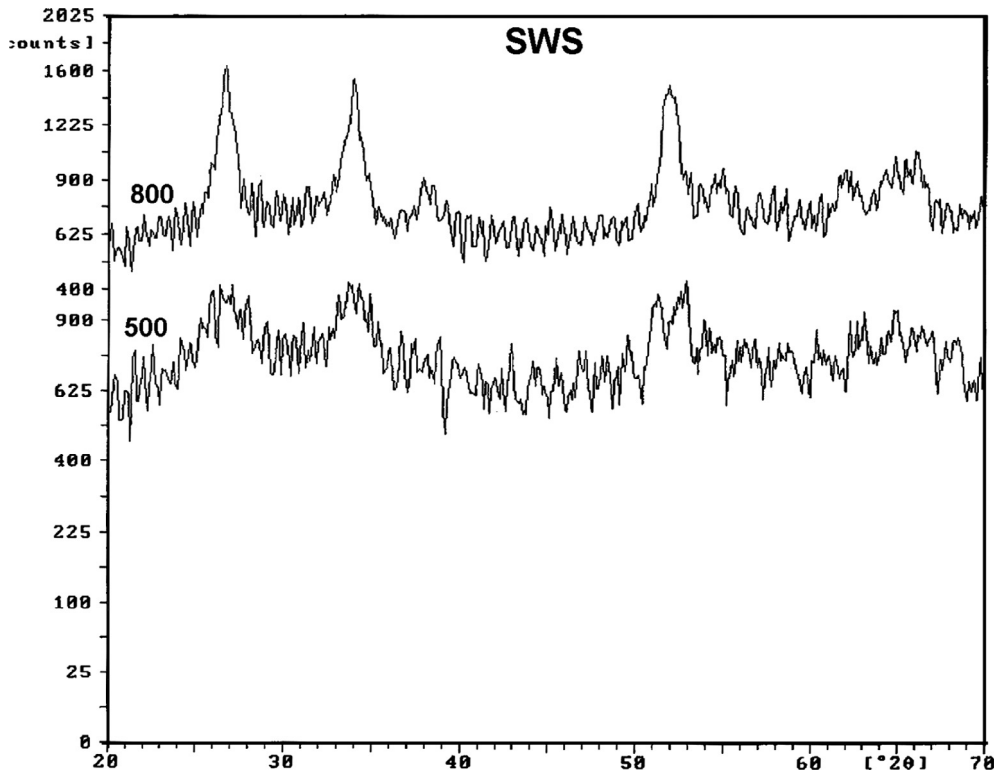

Figure 2 XRD curves of SWS-500 and SWS-800 catalysts.

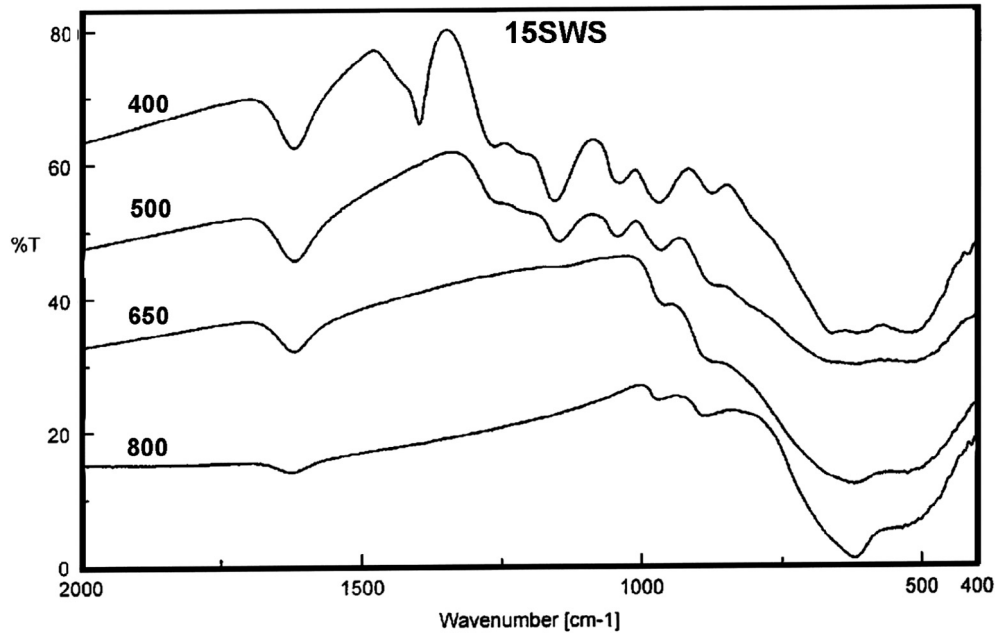

Figure 3 FTIR spectra of SWS catalysts calcined at different temperatures.

3.4. Textural properties

The textural properties such as BET surface area (S_{BET}), total pore volume (V_T), mean pore radius (r_a), micropore volume (V_o) and pore size distribution of SWS catalysts have been evaluated using the nitrogen adsorption – desorption measurements at 77 K in a relative pressure ranging from 0.001 to 0.950. Fig. 4 exhibits the N_2 adsorption–desorption isotherms. The adsorption–desorption of samples calcined at $\leqslant$400 °C are of Type I, indicating that these samples are microporous solids, whereas for $\geqslant$500 °C are of Type VI with hysteresis loops of Type H2 (Sing et al., 1985) indicating that these

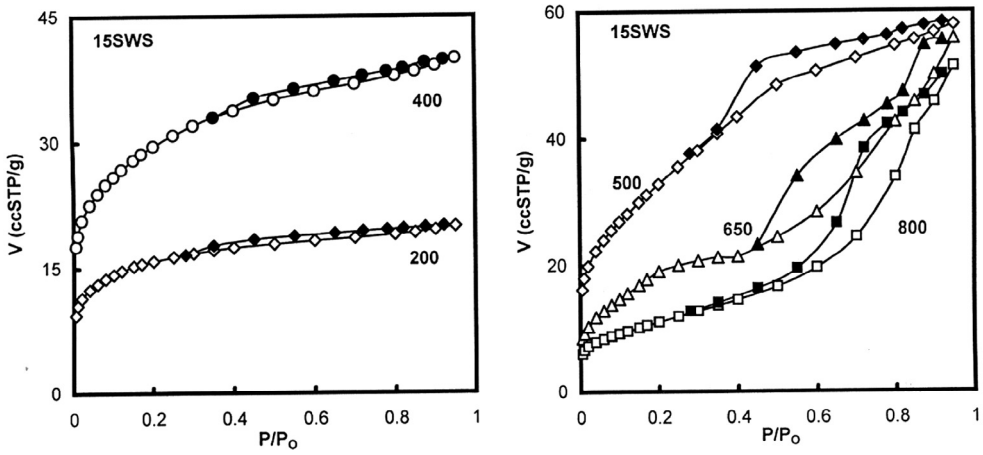

Figure 4 Adsorption isotherms of nitrogen at 77 K on SWS catalysts.

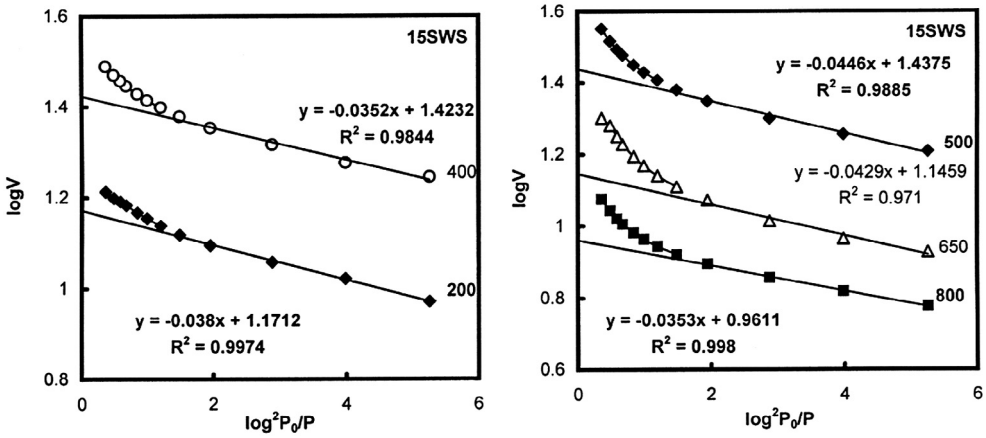

Figure 5 The DR plots for SWS catalysts.

samples are mesoporous solids. The hysteresis loops are closed at $P/P_o \geqslant 0.4$. The S_{BET} values were determined from the analysis of nitrogen adsorption data according to Brunaur–Emmett–Teller (BET method) (Brunaur et al., 1938). It is found that the linear plots are in the range of $P/P_o = 0.02$–0.30 for the $\geqslant$500 °C products, whereas for $\leqslant$400 °C samples are less (0.02–0.25) due to the presence of micropores. The total pore volume values are taken from the amount of N_2 adsorbed at $P/P_o = 0.95$ in liquid form. The r_a values are calculated from the equation:

$$r_a(\text{nm}) = 2000 V_T / S_{BET}$$

The V_o values are estimated from applying Dubinin–Radushkevich equation (Gregg and Sing, 1982):

$$\log V = \log V_o - \text{D} \log^2 P_o/P$$

where V represents the volume of N_2 adsorbed at P/P_o, and D is the Dubinin constant. Fig. 5 shows the DR plots of the SWS catalysts. It is obvious that the DR plots show upward deviations at $P/P_o \geqslant 0.04$, and the deviation increased with an increase in the calcination temperature, which means that the catalysts contain wide micropores as well as mesopores.

Table 1 The textural properties of prepared catalysts.

Sample	C_{BET}	S_{BET} (m^2/g)	V_T (ml/g)	r_a (nm)	i_o (ml/g)	V_o/V_T (%)
SWS-200	304	56.96	0.0309	1.09	0.0229	74.11
SWS-400	192	106	0.0617	1.16	0.0410	66.45
SWS-500	75	120	0.0895	2.38	0.0424	47.37
SWS-650	67	67.45	0.0861	2.55	0.0216	25.09
SWS-800	99	39.92	0.0793	3.97	0.0141	17.78

Table 1 summarizes the textural properties of the prepared samples.

Examination of Table 1 shows the following: (i) The S_{BET}, V_T and V_o values are increased with raising the calcination temperature to show maxima at 500 °C, after that they decreased gradually. The loading of hydrous stannia with WO_3 and SO_4^{2-} inhibits sintering. Also, the loss of chemically bonded water and dehydroxylation leads to the increase of surface area and porosity up to 500 °C, whereas the decomposition of sulfate species bonded to the surface and crystallization of WO_3 and SnO_2 at $>$500 °C lead to a decrease in these textural properties. (ii) The mean pore radii are in the range of microp-

ores for $\leqslant$400 °C products and in the range of mesopores for $\geqslant$500 °C products. The r_a is increased gradually with an increase in the calcination temperature. (iii) The percentage of microporosity (V_o/V_T) decreased gradually with an increase in the calcination temperature. The loss of water and an increase in the crystallinity would cause widening of the pores.

The pore size distribution curves ($\Delta V_p/\Delta r_p$ against r_p) for the $\geqslant$500 °C products were calculated through Orr and Dalla Valle method (Gregg and Sing, 1982) from the desorption branches of the isotherms, Fig. 6. It is observed from this figure that the pore size distribution curves show main peaks in the range of mesoporosity at 1.58, 2.12 and 3.13 nm for SWS-500, SWS-650 and SWS-800 catalysts, respectively. The peak is shifted to higher mean pore radius with an increase in calcination temperature. The values of r_p are in good agreement with r_a values.

3.5. Surface acidity measurements

The surface acidity measurements of the prepared catalysts by means of potentiometric titration with *n*-butylamine in acetonitrile (Bennaradi et al., 2007) were used to estimate the amount of acid sites and their relative acid strength according to the value of the initial electrode potential (E_i). *n*-butylamine is a strong base and can be adsorbed on acid sites of different strength and types, thus it titrates both Lewis and Brønsted sites (Tanabe, 1981). On the other hand, the acid strength of these sites may be classified according to the following scale (Cid and Pecchi, 1985; Sharma et al., 2004): $E_i > 100$ mV (very strong sites), $0 < E_i < 100$ mV (strong sites), $-100 < E_i < 0$ mV (weak sites) and $E_i < -100$ mV (very weak sites). Fig. 7 shows the titration curves obtained for the calcined catalysts. The computed amount of the acid sites (mmol/g) and the number of the acid sites per m^2 (N/m^2) as well as the values of E_i are listed in Table 2. For comparison, the surface acidity of WS-400 catalyst is represented in the Table.

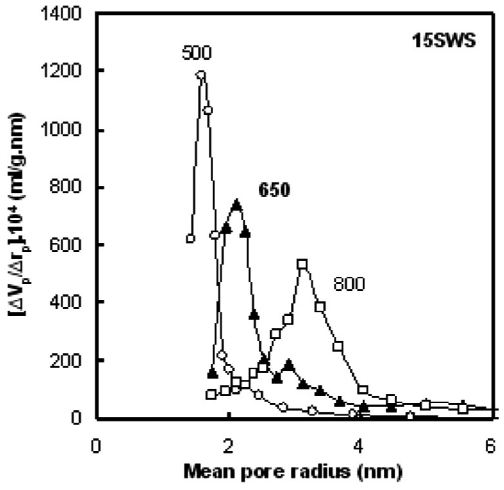

Figure 6 Pore size distribution from N_2 desorption data for SWS catalysts.

The results of surface acidity measurements reveal the following points: (i) All the samples presented very strong acid sites, with E_i values in the range of 337–530 mV. The loading of WS with sulfate ions enhances the acid strength of the catalyst. The maximum acid strength is for the catalyst calcined at 500 °C. (ii) The calcination of SWS catalyst at 400 °C causes a sharp decrease in the amount of acidity due to the loss of some hydrogen ions (Brønsted sites) as water by combination with OH groups. (iii) The raising the calcination temperature from 400 to 800 °C causes a gradual decrease in the amount and number of acid sites, due to hydroxylation and decomposition of sulfate species on the support surface. (iv) The loading of WS catalyst with sulfate ions causes a remarkable increase of surface acidity. Since the amount of acidity and N/m^2 for WS-400 catalyst are 0.0203 mmol/g and $0.924 \times 10^{17}/m^2$, whereas for SWS-400 catalyst are 0.970 mmol/g and $55.12 \times 10^{17}/m^2$, respectively.

The FTIR spectra of adsorbed pyridine on the catalyst surface are shown in Fig. 8. The spectra of the calcined samples show a characteristic band at 1486 cm^{-1} attributed to the adsorption of pyridine on Brønsted or/and Lewis acid sites (Alaya and Rabah, 2008; Khder and Ahmed, 2009; Tyagi et al., 2009). The spectra show bands and shoulders at 1457, 1508, 1558 and 1623 cm^{-1} which are attributed to the pyridine adsorbed on Lewis acid sites (Tanabe, 1981; Villabrille et al., 2002; Rao et al., 2006). The bands at 1538 and 1634 cm^{-1} are due to the pyridine adsorbed on Brønsted acid sites with

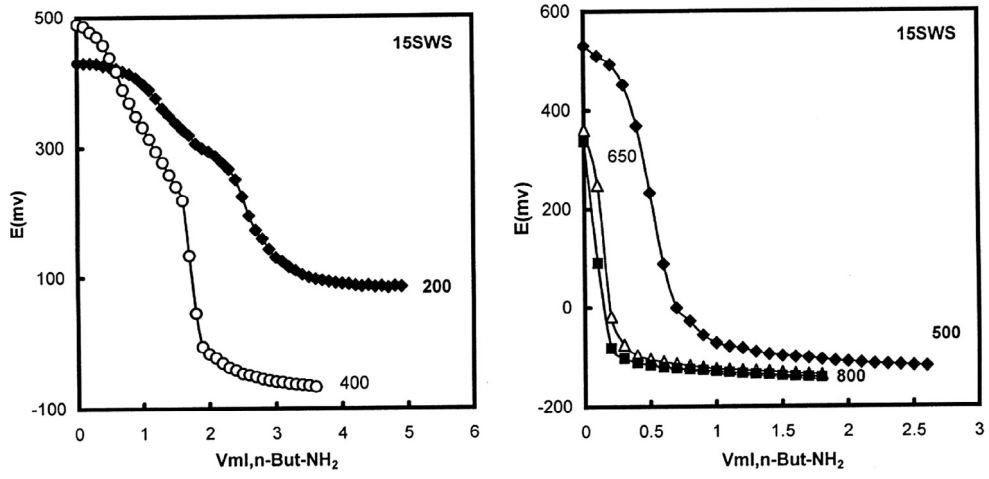

Figure 7 Potentiometric titration curves of SWS catalysts.

Table 2 The surface acidity of SWS catalysts.

Sample	S_{BET} (m^2/g)	E_i (mV)	Acidity amount (mmol/g)	Acid sites number/m^2 (N/m^2) 10^{-17}
SWS-200	57.0	430	2.960	312.9
SWS-400	106	489	0.970	55.12
SWS-500	120	530	0.365	18.32
SWS-650	67.5	361	0.125	18.86
SWS-800	39.95	337	0.055	4.911
WS-400	132	106	0.020	0.924

the formation of pyridinum ion (Tanabe, 1981; Villabrille et al., 2002; Pizzio et al., 2003; Khder and Ahmed, 2009). The SWS-400 catalyst shows bands at 1400–1440 cm^{-1} due to the pyridine adsorbed by hydrogen bonds (Maksimov et al., 2000; Pizzio et al., 2003). These bands disappeared completely with raising the calcination temperature to $\geqslant 500$ °C. The intensities of all bands decreased sharply with an increase in the calcination temperature due to dehydroxylation and decomposition of sulfate species. The generation of strong Lewis acidity by sulfate species may be due to the presence of surface complexes which has a covalent S=O bond, that act as electron-withdrawing species followed by the inductive effect. This effect makes the Lewis acid strength of Sn^{4+} stronger (Furuta et al., 2004). On addition, the presence of water molecules or OH-surface groups on the surface of the catalyst gives Brønsted acid sites, and the adsorption of water molecule would convert Lewis acid sites to Brønsted acid sites. The presence of SO_4 on WO_3/SnO_2 followed by calcination would cause changes in textural and acidic properties of the support since SO_4 may be bonded directly to the surface of SnO_2 or to WO_6 surface species. The calcination at > 500 °C shows loss of the textural properties and acidity that is probably due to the agglomeration of crystalline WO_3 on the surface of SnO_2, decomposition of sulfate species and sintering effect.

3.6. Catalytic activity

The esterification of carboxylic acid with various alcohols is an electrophilic substitution reaction. The reaction is relatively slow and needs activation by acid catalyst, Brønsted acid (Lilja et al., 2002; Sharma et al., 2004) or Lewis acid (Rao et al., 1979; Khder et al., 2008). In general, the esterification reaction is dependent on: (i) temperature of the reaction, (ii) catalyst amount, (iii) proportion of the reactants, (iv) stirrer speed and (v) pressure of operation (Rao et al., 1979). It was found in the esterification of propionic acid (PA) with *n*-butanol (B) and other alcohols that the conversion of the acid was independent of stirrer speed except at 100 rpm since the external diffusion limitation is negligible at stirrer speeds of 200 rpm and above (Ali et al., 2007). Therefore, a stirrer speed of 600 rpm was maintained during all the experiments.

3.6.1. Effect of reaction time

The influence of reaction time on PA conversion is given in Fig. 9 using SWS-400 catalyst under the reaction conditions: 0.2 g catalyst, molar ratio A:B = 1:2 at 110 °C. A gradual increase in the conversion is observed with the increase in the duration of the reaction period. As seen from Fig. 9, in 2 h of the reaction time 80.48% of conversion was obtained, and in 4 h the conversion was 86.58%, whereas at the end of 6 h only 87.24% of the reaction was completed. The selectivity toward *n*-butyl propionate on the other hand remains the same, i.e. 100%. This suggests that 4 h is sufficient to optimize the reaction parameters.

Kinetic data reported on esterification of propionic acid with *n*-butanol are relatively scarce in the open literature. Study of this reaction in a stirred reactor using sulfuric acid as catalyst (Venkateswarlu et al., 1976), sulfuric acid and $AlCl_3$ (Rao et al., 1979) and cation exchange resins (Liu and Tan, 2001) indicates that the reaction obeys a second order equation with respect to propionic acid concentration. The kinetic data

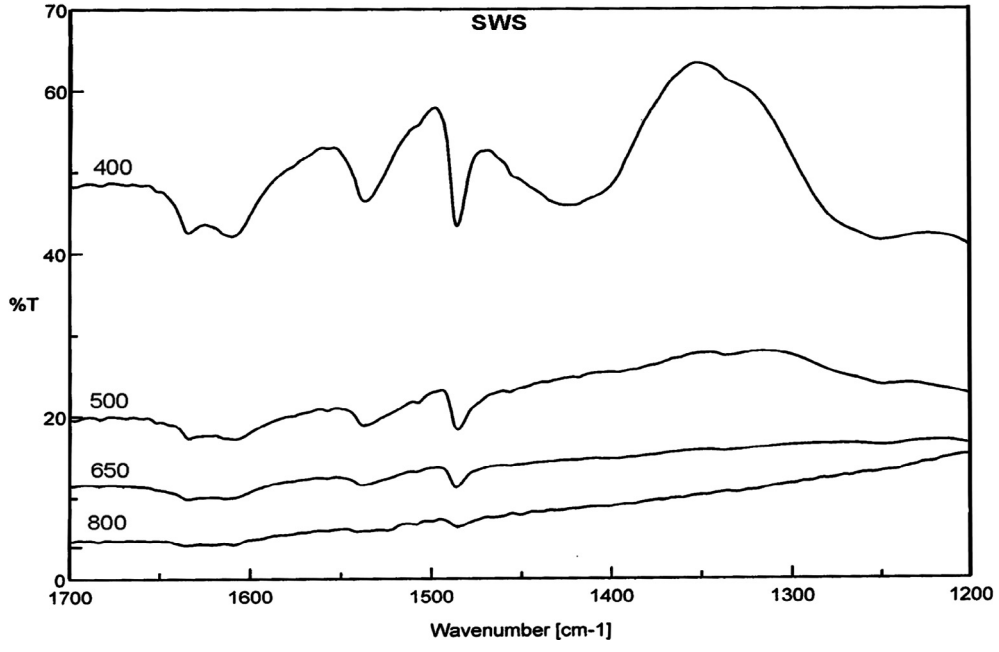

Figure 8 FTIR spectra of pyridine adsorbed on SWS catalysts calcined at different temperatures.

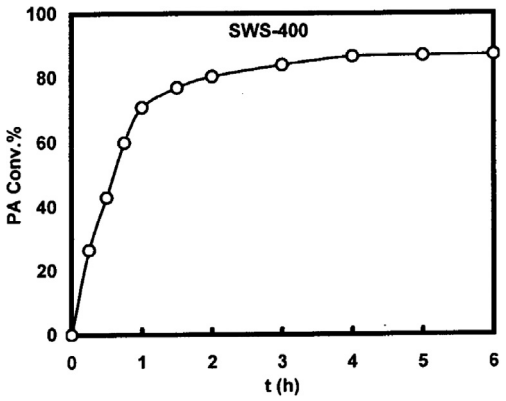

Figure 9 Effect of reaction time on the PA conversion over SWS-400 catalyst.

of this reaction using SWS-400 catalyst are shown in Fig. 10. The plot of 1/[PA] with time is linear over a considerable range of conversion, up to 2 h. The slope of linear line is a measure of the specific reaction rate constant, which is calculated to be $k = 0.54925\ M^{-1}h^{-1}$.

3.6.2. Effect of reaction temperature

The reaction was studied over SWS-400 catalyst at reaction temperatures between 70–110 °C. The conditions of the reaction were: the molar ratio acid/alcohol equal to 1:2, the weight of the catalyst was 0.2 g and the time of reaction was 4 h. The percentage conversion of propionic acid at different reaction temperatures are given in Table 3. It is obvious that the conversion of PA increases gradually with an increase in the reaction temperature. The increase in the temperature brings more collisions and therefore more successful collisions. These successful collisions have sufficient energy (activation energy) to break the bonds and form products and thus result in higher values of conversion of PA (Ali et al., 2007). On the other hand, the increase in reaction temperature favors the formation of ester (Khder, 2008).

3.6.3. Effect of catalyst amount

The effect of the weight of SWS-400 catalyst (0.05–0.30 g) at 110 °C for a reactant molar ratio A:B = 1:2 and a reaction time of 4 h was studied. The percentage conversion of propionic acid is given in Table 3. It is shown that the PA conversion increased gradually with an increase in the weight of the catalyst from 0.05 to 0.20 g, after that the conversion is constant. The increase of the catalyst weight means more available active sites for this reaction. It appeared that 0.20 g of the catalysts is sufficient to bring the highest conversion of the amount of propionic acid used in the experiment.

3.6.4. Effect of reactant molar ratio

The esterification results of PA with B over 0.2 g SWS-400 catalyst at 110 °C after 4 h with different initial molar ratios of A:B are shown in Table 3. It is clear that an increase of alcohol concentration leads to an increase of the final conversion. The conversion of PA increased remarkably from 42.40% to 70.78% with the decrease of the molar ratio from 2:1 to 1:1. A further decrease in A:B to 1:2 is accompanied with a gradual increase in conversion, after that the increase of conversion is slight when the A:B attained 1:3. The use of excess alcohol is typical in order to shift the equilibrium toward the formation of the ester (Dakshinamurty et al., 1984; Yadav and Thathagar, 2002). Furthermore, a high initial amount of acid has a retarding effect on the esterification kinetics (Lilja et al., 2005).

3.6.5. Effect of calcination temperature

Table 4 and Fig. 11 show the PA conversion over SWS calcined at different temperatures (400–800 °C) at reaction temperatures 90 and 110 °C. The PA conversion over SWS catalysts was decreased with raising the calcination temperature. At 90 °C reaction temperature, the conversion decreased from 80.03% to 62.85% when the calcination temperature rose from 400 to 500 °C, the conversion decreased sharply to 7.58% on 650 °C product, and attains 3.87 on 800 °C product. Whereas at 110 °C reaction temperature, the PA conversion decreased slightly from 86.58% to 83.49% for 400 and 500 °C products, respectively, then decreased gradually with raising the calcination temperature. The remarkable decrease of catalytic activity for calcined products at > 500 °C may be due to the loss of Brønsted acid sites, decomposition of sulfate species and sintering effect. The loading of WS catalyst with sulfate ions causes a remarkable increase in the catalytic activity toward the PA esterification, since the PA conversion on WS-400 attains only 16.2% and 35.67% at 90 and 110 °C, respectively, under the same reaction conditions.

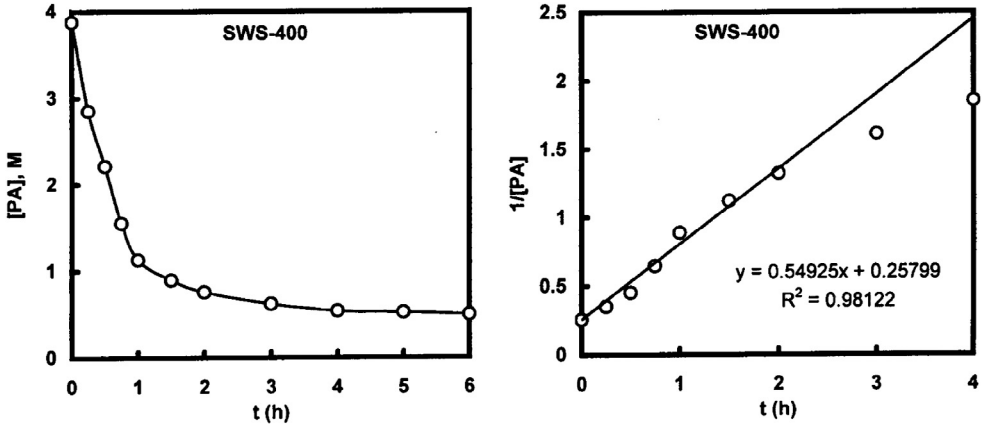

Figure 10 Kinetics of esterification of PA with B over SWS-400 catalyst.

Table 3 The effect of reaction temperature, reactant molar ratio and weight of catalyst on PA conversion.

Reaction temp.(°C)	Con.%*	Molar ratio A:B	Con.%**	Catalyst weight (g)	Con.%***
70	67.49	2:1	42.40	0.05	72.65
80	70.59	1:1	70.78	0.10	82.46
90	80.03	1:2	86.58	0.20	86.58
110	86.58	1:3	87.40	0.30	86.58

* Catalyst weight 0.2 g; A:B = 1:2; reaction time 4 h.
** Reaction temp. 110 °C; catalyst weight 0.2 g; A:B = 1:2; reaction time 4 h.
*** Reaction temp. 110 °C; A:B = 1:2; Reaction time 4 h.

Table 4 Effect of calcination temperature on PA conversion over SWS catalysts.

Calcination temp.(°C)	Con.%*	Calcination temp.(°C)	Con.%**
400	80.03	400	86.58
500	62.85	500	83.49
650	7.58	650	55.11
800	3.87	800	39.11

* Reaction Temp. 90 °C; catalyst weight 0.2 g; A:B = 1:2; reaction time 4 h.
** Reaction Temp. 110 °C; catalyst weight 0.2 g; A:B = 1:2; reaction time 4 h.

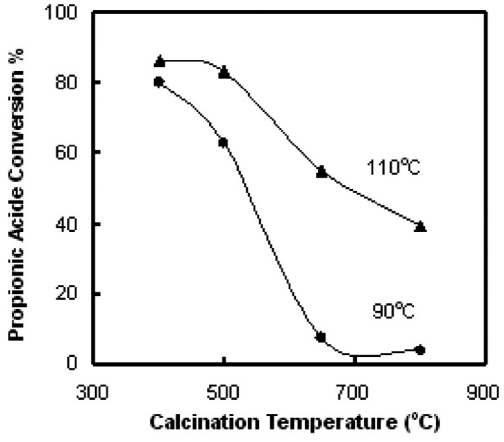

Figure 11 Effect of calcination temperature on the PA conversion over SWS catalyst at RT of 90° and 110 °C.

3.6.6. *Mechanism of the reaction*

The esterification reaction is a straight forward reaction subject to general Brønsted acid catalysis (Liu and Tan, 2001; Sharma et al., 2004; Lilja et al., 2005; Ali et al., 2007). However, according to other authors (Kirumakki et al., 2006; Barbosa et al., 2006) esterification can also be catalyzed by Lewis acid sites. On the other hand, many authors (Wang and Li, 2004; Samantaray and Parida, 2003; Khder et al., 2008) reported that both the Brønsted and Lewis acid sites are responsible for catalyzing the esterification reactions. According to the above results the mechanism of the reaction follows a Rideal–Eley mechanism in which propionic acid molecules are adsorbed

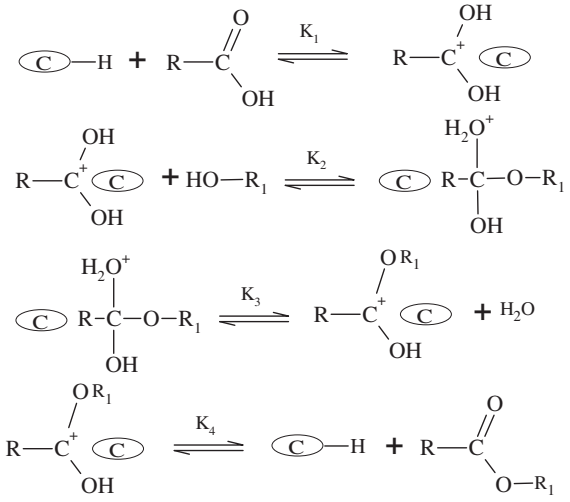

Scheme 1 Reaction mechanism for the esterification of propionic acid with *n*-butanol over Bronsted acid sites. R: CH_3CH_2-; R_1: $CH_3CH_2CH_2CH_2$.

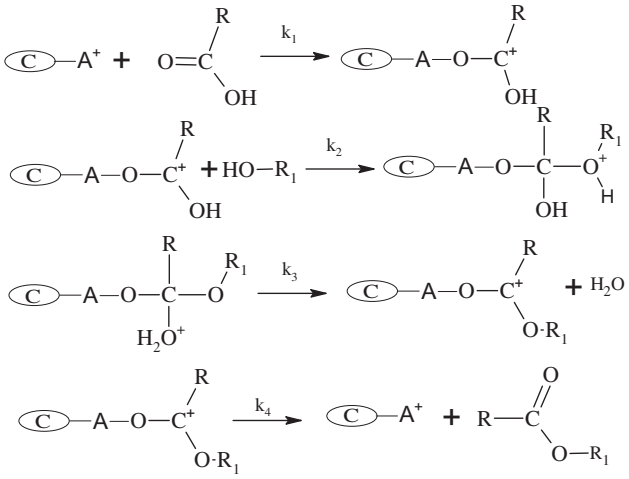

Scheme 2 Reaction mechanism for the esterification of propionic acid with *n*-butanol over Lewis acid sites. R: CH_3CH_2-; R_1: $CH_3CH_2CH_2CH_2$.

on the active sites of the catalyst, Brønsted and Lewis acid sites, forming protonated propionic acid or carbocation intermediate, as shown in Schemes 1 and 2, and then reacted with *n*-butanol molecules from the bulk liquid. The products formed, namely, *n*-butyl propionate and water, are then desorbed from the surface. The adsorption and protonation of PA or carbocation formation on the catalyst surface is assumed to be the rate-controlling step. More details on the derivation of this model can be found in the literature (Lilja et al., 2005; Kirumakki et al., 2006; Khder et al., 2008).

Some authors (Chu et al., 1996; Dash and Parida, 2007; Parida and Mallick, 2007) proposed that the esterification mechanism of *n*-butanol with acetic acid and other carboxylic acids catalyzed by strong Brønsted acid sites proceeds via a protonated alcohol intermediate. The reaction following the Rideal–Eley mechanism takes place between alcohols

chemisorbed on active Brønsted acid sites of the catalyst surface, forming a stable carbocation. Then, the carbocation attacks the nucleophilic center of carboxylic acid to form an unstable intermediate. Removal of a proton from the intermediate gives the final product with the regeneration of the catalyst. The role of an acid catalyst here is to facilitate the formation of the carbocation, and to help remove OH^- from the alcohol.

4. Conclusions

The interaction between sulfate ion and WO_3/SnO_2 affects the physicochemical properties of the prepared catalysts with calcination temperature. XRD results reveal that WO_3 dispersed completely on the surface of SnO_2 and sulfating of WO_3/SnO_2 hinders the crystallization of SnO_2. The textural properties are maxima at 500 °C. The catalysts possess very strong acid sites and contain both Brønsted and Lewis acid sites. The acid strength of acid sites is strongest for 500 °C products, and the total surface acidity decreased with an increase in the calcination temperature. Sulfation enhances the surface acidity and increases the strength of Lewis acidity due to the inductive effect of S═O. The optimum conditions for the formation of the *n*-butyl propionate were observed to be: reaction temperature of 110 °C, molar ratio A:B = 1:2, 0.2 g of the catalyst and reaction time of 4 h. The reaction obeys second order kinetic equation with respect to PA concentration. Brønsted and Lewis acid sites appear to be needed for catalytic activity in *n*-butyl propionate formation.

References

Ai, M., 1984. Dimerization of formaldehyde to methyl formate on SnO_2–WO_3 catalysts. Appl. Catal. 9 (3), 371–377.

Alaya, M.N., Rabah, M., 2008. Study of physicochemical properties of sulfated alumina. Res. J. Aleppo Univ., Basic Sci. Ser. 61, 13–36.

Ali, S.H., Tarakmah, A., Merchant, S.Q., Al-Sahhaf, T., 2007. Synthesis of esters: development of the rate expression for the Dowex 50 W8-400 catalyzed esterification of propionic acid with 1-propanol. Chem. Eng. Sci. 62, 3197–3217.

Arata, K., Hino, M., 1993. Synthesis of solid superacids of tungsten oxide supported on tin oxide, titanium oxide and iron oxide and their catalytic action. In: Guczi, L. et al., (Eds.), New Frontiers in Catalysis, Proceeding of the 10th International Congress on Catalysis, 19–24 July, 1992, Budapest, Hungary, pp. 2613–2616.

Arata, K., 1996. Preparation of superacids by metal oxides for reactions of butanes and pentenes. Appl. Catal. A: Gen. 146, 3–32.

Arata, K., Nakamura, H., Shouji, M., 2000. Friedl–Craft acylation of toluene catalyzed by solid superacids. Appl. Catal. A: Gen. 197, 213–219.

Bahatt, N., Patel, A., 2005. Esterification of 1° and 2° alcohol using an ecofriendly solid acid catalyst comprising 12-tungstosilicic acid and hydrous zirconia. J. Mol. Catal. A: Chem. 238, 223–228.

Barbosa, S.L., Dabdoub, M.J., Huratado, G.R., Klein, S.I., Baroni, A.C.M., Cunha, C., 2006. Solvent free esterification reactions using Lewis acids in solid phase catalysis. Appl. Catal. A: Gen. 313 (2), 146–150.

Bennaradi, D.O., Romanelli, G.P., Autino, J.C., Pizzio, L.R., 2007. Supported trifluromethanesulfonic acid as catalyst in the synthesis of flavone and chromone derivatives. Appl. Catal. A: Gen. 324, 62–68.

Brunaur, S., Emmett, P.H., Teller, E., 1938. Adsorption of gases in multimolecular layers. J. Am. Chem. Soc. 60, 309–319.

Chu, W., Yang, X., Wu, Y., 1996. Vapor phase esterification catalyzed by immobilized dodecatungstosilicic acid (SiW_{12}) on activated carbon. J. Appl. Catal. A: Gen. 145, 125–140.

Cid, R., Pecchi, G., 1985. Potentiometric method for determining the number and relative strength of acid sites in colored catalysts. Appl. Catal. 14, 15–21.

Cui, X., Ma, H., Wang, B., Chen, H., 2007. Direct oxidation of *n*-heptane to ester over modified sulfated SnO_2 Catalysts under mild conditions. J. Hazard. Mater. 147, 800–805.

Dash, S.S., Parida, K.M., 2007. Esterification of acetic acid with *n*-butanol over manganese nodule leached residue. J. Mol. Catal. A: Chem. 266, 88–92.

Dakshinamurty, P., Ramarao, M.V.S., Ramachandramurty, Ch.V., 1984. Kinetics of catalytic esterification of propan-1-ol with propionic acid using cation exchange resin. J. Chem. Technol. Biotechnol. 34A, 257–261.

Furuta, S., Matsuhashi, H., Arata, K., 2004. Catalytic action of sulfated tin oxide for etherification and esterification in comparison with sulfated zirconia. Appl. Catal. A: Gen. 269, 187–191.

Gregg, S.J., Sing, K.S.W., 1982. Adsorption, Surface Area and Porosity, second ed. Acad. Press, London.

Gutierrez-Baez, R., Toledo-Antonio, J.A., Cortes-Jacome, M.A., Sebastian, P.J., Vazquez, A., 2004. Effects of the SO_4 groups on the textural properties and local order deformation of SnO_2 rutile structure. Langmuir 20 (10), 4265–4271.

Hino, M., Takasaki, S., Furuta, S., Matsuhashi, M., Arata, K., 2006. Synthesis of a ceramics acid of tungstated stannia more active than aluminosilicates for the esterification of *n*-octanoic acid with methanol. Catal. Commun. 7, 162–165.

Hino, M., Takasaki, S., Furuta, S., Matsuhashi, M., Arata, K., 2007. Meta-Stannic acid as an effective support for the preparation of sulfated and tungstated stannias. Appl. Catal. A: Gen. 321, 147–154.

Khder, A.S., El-Sharkawy, E.A., El-Hakam, S.A., Ahmed, A.I., 2008. Surface characterization and catalytic activity of sulfated tin oxide catalyst. Catal. Commun. 9, 769–777.

Khder, A.S., 2008. Preparation, characterization and catalytic activity of tin oxide-supported 12-tungstophosphoric acid as a solid catalyst. Appl. Catal. A: Gen. 343, 109–116.

Khder, A.S., Ahmed, A.I., 2009. Selective nitration of phenol over nanosized tungsten oxide supported on sulfated SnO_2 as a solid acid catalyst. Appl. Catal. A: Gen. 354 (1-2), 153–160.

Kirumakki, S.R., Nagaraju, N., Chary, K.V.R., 2006. Esterification of alcohols with acetic acid over zeolites Hβ, HY and HZSM5. Appl. Catal. A: Gen. 299, 185–192.

Lee, M.J., Chiu, J.Y., Lin, H., 2002. Kinetics of catalytic esterification of propionic acid and *n*-butanol over Amberlyst 35. Ind. Eng. Chem. Res. 41, 2882–2887.

Lilja, J., Aumo, A., Salmi, T., Murzin, D.Y., Maki-Arvela, P., Sundell, M., Ekman, K., Peltonen, R., Vainio, H., 2002. Kinetics of esterification of propionic acid with methanol over fibrous polymer-supported sulphonic acid catalyst. Appl. Catal. A: Gen, 228, 253–267.

Lilja, J., Warna, J., Salmi, T., Pettersson, L.J., Ahlkvist, J., Grenman, H., Ronnholm, M., Murzin, D.Y., 2005. Esterification of propionic acid with ethanol, 1-propanol and butanol over a heterogeneous fiber catalyst. Chem. Eng. J. 115, 1–12.

Liu, Y., Lotero, E., Goodwin Jr., J.G., 2006. Effect of carbon chain length on esterification of carboxylic acids with methanol using acid catalysis. J. Catal. 243, 221–228.

Liu, W.T., Tan, C.S., 2001. Liquid-phase esterification of propionic acid with *n*-butanol. Ind. Eng. Chem. Res. 40, 3281–3286.

Ma, Z., Hua, W., Tang, Y., Gao, Z., 2000. Catalytic decomposition of CFC-12 over solid acid WO_3/M_xO_y (M═Ti, Sn, Fe). J. Mol. Catal. A: Chem. 159 (2), 335–345.

Maksimov, G.M., Fedotov, M.A., Bogdanov, S.V., Litvak, G.S., Golovin, A.V., Likholobov, V.A., 2000. Synthesis and study of acid catalyst 30%WO_3/SnO_2. J. Mol. Catal. A: Chem. 158, 435–438.

Matsuhashi, H., Hino, M., Arata, K., 1990. Solid catalyst treated with anion: XIX. Synthesis of the solid superacid catalyst of tin oxide treated with sulfate ion. Appl. Catal 59, 205–212.

Parida, K.M., Mallick, S., 2007. Silicotungstic acid supported zirconia: an effective catalyst for esterification reaction. J. Mol. Catal. A: Chem. 275, 77–83.

Pimtong-Ngam, Y., Jiemsirilers, S., Supothina, S., 2007. Preparation of tungsten oxide-tin oxide nanocomposites and their ethylene sensing characteristics. Sens. Actuat. A 139, 7–11.

Pizzio, L.R., Vazquez, P.G., Caceres, C.V., Blanco, M.N., 2003. Supported Keggin type heteropolycompounds for ecofriendly reactions. Appl. Catal. A: Gen. 256, 125–139.

Rao, B.A., Raghavaiah, C.V., Reddy, M.S., Chiranjivi, C., 1979. Esterification of 1-butanol with propionic acid in a stirred tank batch reactor. Chem. Petro-Chem. J., 7–12.

Rao, K.N., Reddy, K.M., Lingaiah, N., Suryanarayana, I., Prasad, P.S.S., 2006. Structure and reactivity of zirconium oxide-supported ammonium salt of 12-molybdophosphoric acid catalysts. Appl. Catal. A: Gen. 300, 139–146.

Salavati-Niasari, M., Mmir, N., Davar, F., 2010. Synthesis, characterization and optical properties of tin oxide nanoclusters prepared from a novel precursor via thermal decomposition route. Inorgan. Chimica Acta 363 (8), 1719–1726.

Samantaray, S.K., Parida, K., 2003. SO_4^{2-}/TiO_2–SiO_2 mixed oxide catalyst, 3. An eco-friendly catalyst for esterification of acetic acid. React. Kinet. Catal. Lett. 78, 381–387.

Sarkar, A., Ghosh, S.K., Pramanik, P., 2010. Investigation of the catalytic efficiency of a new mesoporous catalyst SnO_2/WO_3 towards oleic acid esterification. J. Mol. Catal. A: Chem. 327, 73–79.

Sharma, P., Vyas, S., Patel, A., 2004. Heteropolyacid supported onto neutral alumina: characterization and esterification of 1° and 2° alcohol. J. Mol. Catal. A: Chem. 214 (2), 281–286.

Shouli, B., Dianqing, L., Dongmei, H., Ruixian, L., Aifan, C., Liu, C.C., 2010. Preparation, characterization of WO_3–SnO_2 nanocomposites and their sensing properties for NO_2. Sens. Actuat. B: Chem. 150, 749–755.

Sing, K.S.W., Everett, D.H., Haul, R.A.W., Mosco, L., Pierotti, R.A., Rouquerol, J., Sieminiewska, T., 1985. Reporting physisorption data for gas/solid systems with special reference to the determination of surface area and porosity. Pure Appl. Chem. 57 (4), 559–603.

Sohn, J.R., Lee, S.H., Lim, J.S., 2006. New solid superacid catalyst prepared by doping ZrO_2 with Ce and modifying with sulfate and its catalytic activity for acid catalysis. Catal. Today 116 (2), 143–150.

Tanabe, K., 1981. Solid acid and base catalysts. In: Anderson, J.R., Boudart, M. (Eds.), . In: Catalysis Science and Technology, vol. 2. Springer-Verlag, Berlin Heidelberg and New York, pp. 231–273, Ch. 5.

Tyagi, B., Mishra, M.K., Tasra, A., 2009. Solvent free synthesis of 7-isopropyl-1, 1-dimethyltetralin by the rearrangement of longifolene using nanocrystalline sulfated zirconia catalyst. J. Mol. Catal. A: Chem. 301, 67–78.

Venkateswarlu, K., Sinha, R., Rao, R.J., 1976. Kinetics of esterification of *n*-butanol with propionic acid in a stirred tank batch reactor. Chem. Petrochem. J. Dec, 3–7.

Villabrille, P., Vazques, P., Blanco, M., Caceres, C., 2002. Equilibrium adsorption of molubdosilicic acid solution on carbon and silica: basic studies for the preparation of ecofriendly acidic catalysts. J. Coll. Interf. Sci. 251, 151–159.

Wang, Y., Li, W., 2004. Kinetics of acetic acid esterification with 2-ethoxyethanol over an Al-pillared clay catalyst. React. Kinet. Catal. Lett. 83, 195–203.

Xi, L., Cao, S., 2010. Preparation and characterization of the SBA-8-SO_3H mesoporous molecular sieve functionalized with sulfonic acid in the synthesis of *n*-butyl propionate. React. Kinet., Mech. Catal. 100 (1), 175–185.

Yadav, G.D., Thathagar, M.B., 2002. Esterification of maleic acid with ethanol over cation exchange resin catalysts. React. Funct. Polymers 52, 99–110.

Yamaguchi, T., Jin, T., Tanabe, K., 1986. Structure of acid sites on sulfur-promoted iron oxide. J. Phys. Chem. 90 (14), 3148–3152.

Yamaguchi, T., 1990. Recent progress in solid superacid. Appl. Catal. 61, 1–25.

Zhang, J., Gao, L., 2004. Synthesis and characterization of nanocrystalline tin oxide by sol-gel method. J. Solid State Chem. 177, 1425–1430.